

Nanoscale precision of 3D polymerisation via polarisation control

Sima Rekštytė,[†] Tomas Jonavičius,[†] Darius Gailevičius,[†]
Mangirdas Malinauskas,^{*,†} Vygantas Mizeikis,[‡] Eugene G. Gamaly,[¶] and
Saulius Juodkazis^{*,§,||}

*Laser Research Center, Department of Quantum Electronics, Physics Faculty, Vilnius University,
Saulėtekio Ave. 10, LT-10223, Vilnius, Lithuania, Research Institute of Electronics, Shizuoka
University, 3-5-3-1 Johoku, Naka-ku, Hamamatsu 432-8561, Japan, Research School of Physics
and Engineering, Australian National University, Acton ACT 2601, Australia, Center for
Micro-Photonics, Faculty of Engineering and Industrial Sciences, Swinburne University of
Technology, Hawthorn, VIC, 3122, Australia, and Melbourne Center for Nanofabrication,
Australian National Fabrication Facility, Clayton, VIC 3168, Australia*

E-mail: mangirdas.malinauskas@ff.vu.lt; sjuodkazis@swin.edu.au

^{*}To whom correspondence should be addressed

[†]Laser Research Center, Department of Quantum Electronics, Physics Faculty, Vilnius University, Saulėtekio Ave. 10, LT-10223, Vilnius, Lithuania

[‡]Research Institute of Electronics, Shizuoka University, 3-5-3-1 Johoku, Naka-ku, Hamamatsu 432-8561, Japan

[¶]Research School of Physics and Engineering, Australian National University, Acton ACT 2601, Australia

[§]Center for Micro-Photonics, Faculty of Engineering and Industrial Sciences, Swinburne University of Technology, Hawthorn, VIC, 3122, Australia

^{||}Melbourne Center for Nanofabrication, Australian National Fabrication Facility, Clayton, VIC 3168, Australia

Abstract

A systematic analysis of polarization effects in a direct write femtosecond laser 3D lithography is presented. It is newly shown that coupling between linear polarization of the writing light electric field and temperature gradient can be used to fine-tune feature sizes in structuring of photoresists at a nanoscale. The vectorial Debye focusing is used to simulate polarization effects and a controlled variation up to $\sim 20\%$ in the linewidth is shown experimentally for the identical axial extent of the polymerised features. The revealed mechanisms are relevant for a wide range of phenomena of light-matter interaction at tight focusing in laser-tweezers and in plasmonic or dielectric sub-wavelength focusing where strong light intensity and thermal gradients coexist.

Keywords: femtosecond pulses, laser nanolithography, optical 3D printing, polarization, voxel aspect ratio

Direct laser writing (DLW) is widely used for three-dimensional (3D) material processing and printing. One of its realizations via polymerization enables free-form fabrication of micro-/nano-objects down to tens-of-nanometers in spatial resolution.¹⁻⁴ DLW in polymers is based on curing a resist (resin) by nonlinear absorption at the focal volume of a tightly-focused high peak power pulsed laser radiation. Only a very small volume, which can be sub-100 nm in cross sections, around the focal spot is affected during the pulsed exposure.⁵⁻⁷ Pure optical light delivery at tight focusing cannot explain the final size of the structure due to the threshold effect of laser modification via polymerization/cross-linking, thermal effects within the 3D focal volume, and wet chemistry development which all affect the final shape and size of the 3D structure.⁸⁻¹² Heat accumulation at focus defined by pulse repetition rate and scan speed is used to increase productivity of 3D polymerization and makes thermal issues very important and actively debated.¹³⁻¹⁵ Polarization effects in laser fabrication in 2D and 3D geometries are now explored in polymerization by DLW.¹⁶⁻¹⁹ Also, stimulated-emission-depletion (STED) control of 3D focal volume,^{20,21} orientation of deposition of self-organized materials,^{22,23} melting and oxidation of thin films,²⁴ laser

ablation,^{25,26} and as self-organized nano-patterns induced on surface²⁷ are among other polarisation related phenomena demonstrated recently.

Here a systematic analysis via modeling and experiments is presented to reveal polarization effects, their influence on the feature size (resolution), and the coupling between thermal gradient and polarisation in DLW.

To study and demonstrate the polarisation effects, the 3D suspended resolution bridges at various angles, α , between the linear polarisation and scanning direction were fabricated on a glass substrate (Fig. 1 inset in (a); see details in the Experimental section). The difference of the line widths was 10 - 20% (varying exposure) at typical polymerization conditions for the linearly polarized pulses. The largest width of a 3D bridge was observed when scan direction was perpendicular to the orientation of linear polarization, $\alpha = \pi/2$ ($\mathbf{E} \perp \mathbf{v}_s$). The height-to-width ratio of the suspended lines was dependent on orientation of linear polarization and was changing from 3.07 to 3.44, a self-focusing was not present at our experimental conditions.¹ Detailed analysis of polarisation, threshold, and heat accumulation effects which are all important are discussed next.

There are known effects of polarization on the scalar parameters of laser-matter interaction, such as absorption coefficient and ionization rate.²⁸⁻³¹ It is also known that heat conduction flux (vector) in plasma might be depending on the direction of imposed field.³² In what follows these effects are considered in succession: *(i)* the accumulation from the multiple pulses, *(ii)* effects of polarization under high-NA focusing, and *(iii)* influence of the external high frequency electric field on the electronic heat conduction. The later contribution has not yet been considered in laser fabrication under tight focusing. All these photomodification mechanisms occur simultaneously and affect polymerization which takes approximately a millisecond for common photoresists³³ at a $> 90\%$ voxel overlap at typical writing velocity of $100\mu\text{m/s}$ for widespread laser 3D nanolithography.³⁴

For the used experimental conditions the focal spot diameter (at $1/e^2$) can be calculated as

¹It was checked that the use of VIS-corrected (400 - 700 nm) microscope objective lenses for the IR (1030 nm) laser radiation was not causing additional spherical aberrations and was not increasing the aspect ratio of polymerized bridge lines. The aspect ratio at 515 nm wavelength was 3.00-3.57, almost the same as for 1030 nm case (3.07-3.44) varying polarization direction at intermediate exposure power/intensity.

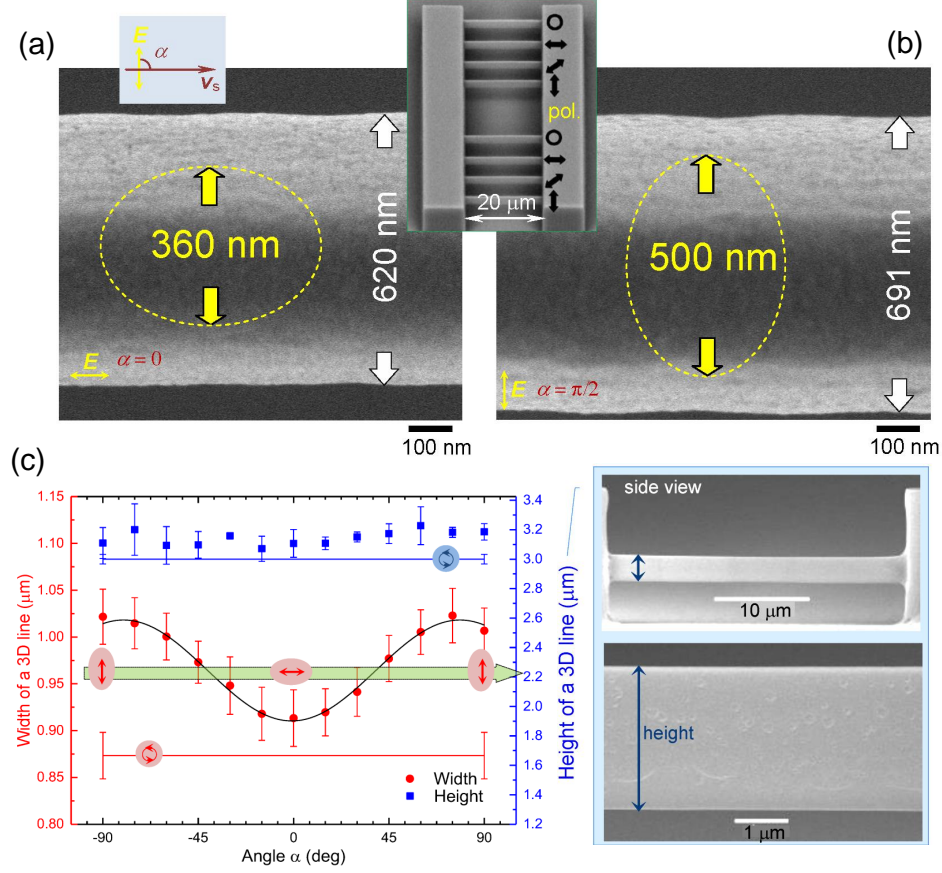


Figure 1: (a-b) Top-view SEM images of 3D suspended bridges formed out of SZ2080 with 1% BIS photo-initiator at the same conditions (scanned along the x-axis at velocity \mathbf{v}_s) except for light polarization direction: $\mathbf{E} \parallel \mathbf{v}_s$ (or angle $\alpha = 0^\circ$) and $\mathbf{E} \perp \mathbf{v}_s$ (or angle $\alpha = 90^\circ$). The width difference is 10.3% for $NA = 1.4$ and $\lambda = 1030$ nm. The ovals show the FWHM intensity cross section calculated by vectorial Debye formula $W_l \times W_s \equiv 500 \times 360$ nm (see Appendix A for details). Note, the heat accumulation due to difference of number of pulses per diameter is $T_N^{\text{long}}/T_N^{\text{short}} = 1.59$. The inset shows a typical SEM image used for determination of the height of the structures; $\text{height}/\text{width}$ from ≈ 3.07 to 3.44 . (c) The width and height of 3D suspended bridges at different angles, α , between scan direction and linear polarization. Numerical aperture $NA = 1.4$, pulse energy $E_p = 0.97$ nJ (at the focus) at 200 kHz repetition rate. The fit line to width data is plotted as $\sim \sin(\phi)$; arrow marks direction of scan.

$d_f = 1.22\lambda/NA = 898$ nm assuming Gaussian intensity profile for simplicity. However, at such tight focusing the vectorial Debye theory (the specifics³⁵ can be found in Appendix A) has to be used which predicts an ellipsoidal focal spot with two lateral cross sections: $W_l = 790$ nm and $W_s = 572$ nm for long and short cross sections, respectively (or 500 and 360 nm at FWHM) for the actual experimental conditions and a sin-apodisation function typical for commercial objective

lenses.

The dwell time of each pulse at the focal spot of diameter, d_f , equals to $t_{dw} = d_f/v_{scan}$. Thus the number of pulses per spot at the repetition rate $R_{rep} = 2 \times 10^5$ pulses/s equals to $N_{spot} = t_{dw} \times R_{rep}$. Heat diffusion coefficient for cold resist is similar to that in silica, $D_{diff} = 10^{-3} \text{ cm}^2/\text{s}$.³⁶ Thus, the cooling time of the heated volume, $t_{th} = d_f^2/D$, has to be compared with the time gap between subsequent pulses - $5 \mu\text{s}$. The heat transfer to the surrounding cold material between the pulses results in the average temperature drop at the arrival of the next pulse and the temperature accumulation can be explicitly calculated for the N pulses as:³⁷

$$T_N = T_1(1 + \beta + \beta^2 + \dots + \beta^N) = T_1 \frac{1 - \beta^N}{1 - \beta}, \quad (1)$$

where $\beta = \sqrt{\frac{t_{th}}{t_{th} + 1/R_{rep}}}$. Assuming the same temperature jump, $T_1 = \text{const}$, for one pulse regardless polarization the accumulation for the two orientations of polarization with respect to the scan direction at fixed speed $v_s = 100 \mu\text{m/s}$ should result in significant differences in heat accumulation: $T_N \simeq 6.39T_1$ ($\alpha = 0$; Fig. 1(b)) along W_1 direction and $T_N = 4.02T_1$ ($\alpha = \pi/2$ along W_s) due to different number of overlapping pulses N . However, in the performed experiments the expected difference of the line widths up to $\sim 59\%$ was not observed and was up to 20% (applying highest, near optical damage intensities) whereas about 10% was a typical deviation (applying intermediate intensities, commonly used for routine DLW lithography fabrication). This matches the previously reported findings that the shrinkage of polymerized features is conversely proportional to the applied exposure power (intensity).³⁸

It was found theoretically that the polarization state affects the shape of the focal spot when the laser beam focuses with high-NA lenses.^{16,40} Effect starts at $NA = 0.2$ and at 0.95 it is significant however not quantified.⁴⁰ The energy density distribution, $w_{en} = (\mathbf{E} \cdot \mathbf{E}^*)/16\pi$ of linearly polarized beam has an elliptical form with the long axis in the E-field direction (Fig. 2(a)). Besides in the central part of the tightly focused beam the polarization state becomes unidentifiable.

The high-NA focusing and polarization around the focal spot of p-polarized (parallel to the

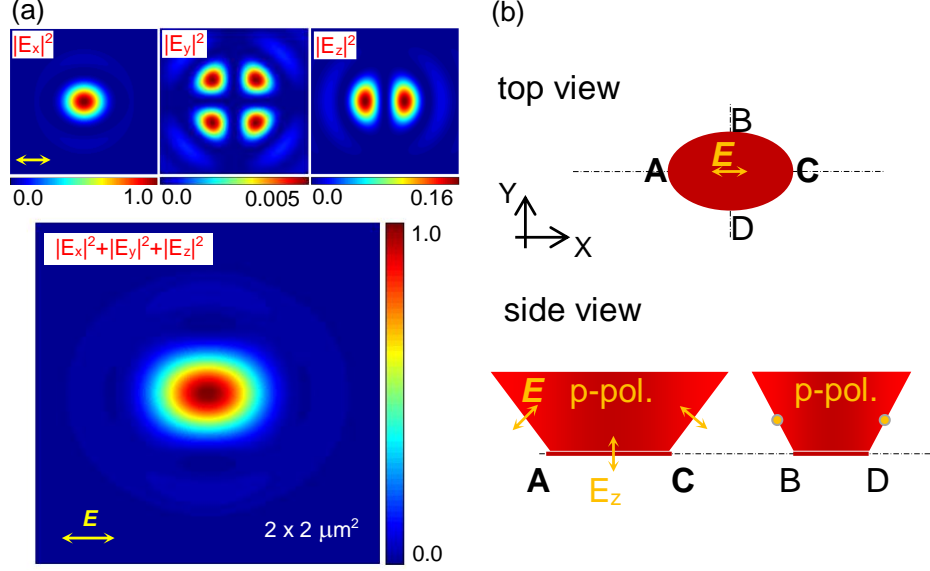


Figure 2: (a) The calculated focal intensity distribution of a linearly x-polarized 1030 nm wavelength beam under $NA = 1.4$ focusing using vectorial Debye theory with sin-apodization function (see Appendix A for details);³⁹ normalized squares of components of E-field (top row) and their sum (bottom row). E-field polarization of the incident light is shown by arrows. (b) Schematic view of polarization under tight focusing, which acquires p- and s-polarization and longitudinal E_z components.

plane of incidence) beam are considered next (Fig. 2(b)). One can see that in the direction $A - C$ (plane of incidence) across the focus polarization changed projection with increased contribution of a perpendicular to the sample surface component and is different from the projection in the $B - D$ cross section. This effect significantly increases for dense plasma for large angle of incidence.⁴¹ The p-pol. always has a stronger absorption in a resist at pre-breakdown conditions while the beam of circular polarization should experience an average absorption of that between s- and p-polarizations (See Appendix B for details).

The difference in the energy absorption along the polarization direction \parallel might be significantly higher than in the perpendicular direction \perp resulting in elongation of the absorbing area in the direction of the field as it was observed in the experiments. It is noteworthy that due to the presence of both lateral E_x and E_y fields (Fig. 2(a)) the p-pol. will be always present at the focal plane (Appendix B).

Analysis presented above shows how to account for polarisation defined absorption which,

in turn, defines local temperature in the focal region. Following a general description, the heat conduction flux in plasma placed into external electro-magnetic field has a form:³²

$$q_\alpha = -\kappa_{\alpha\beta} \frac{\partial T}{\partial x_\beta} = \kappa_1 \frac{\partial T}{\partial x_\alpha} + \kappa_2 \mathbf{e}_\alpha \mathbf{e}_\beta \frac{\partial T}{\partial x_\beta}. \quad (2)$$

The first term is the conventional heat flow, while the second term relates to the contribution due to the effect of external field. Here, $\mathbf{e} = \mathbf{E}/E$ is the unit vector in the direction of the electric field; $\kappa_{1,2}$ are two scalar functions, which can be obtained from the solution of the kinetic equation. Note that the general form of Eqn. 2 is applicable to the constant external field as well as to the high frequency field. The second term contribution holds after averaging over the period of the light oscillation. Thus, it is applicable to the experiments on polymerization by DLW. It follows from Eqn. 2 that the field-related second term equals to zero when the polarization direction is \perp to the temperature gradient, i.e. $\mathbf{e}_x \mathbf{e}_y \equiv 0$. Let us now consider effects of linear and circular polarizations in laser-plasma interactions.

Stationary case. Movement of the laser spot creates different temperature gradients ∇T along and across the scan direction \mathbf{v}_s . It is instructive to consider the most simple case of uniform heated spot and coupling of heat transport with polarization as follows from Eqn. 2 even without scanning.

Linear polarization. The intense laser beam along the normal (z coordinate) produces plasma spot elongated in direction of polarization (x,y plane) at focus, surrounded by a cold unperturbed resist. Let us suggest that the temperature is homogeneous in the interior of the focus. Therefore the temperature gradients are concentrated at the outer boundary of heated spot directed along the radii from the center to the outside; polarization is linear with the \mathbf{E} -field direction along x-axis. As it follows from Eqn. 2 the field affects the heat flow only along the x-axis, while in the other parts of heated circle the heat flow is unperturbed because temperature gradient and the field are perpendicular to each other. Therefore expected effect of the linear polarization is an elongation of the laser-affected spot in the polarization direction turning a circle into an oval.

Circular polarization. The electric field vector of the incident beam at any moment of time is

collinear to the temperature gradient directed along the radius of the beam. Thus, the field influence on a heat flow is evenly distributed along the circle embracing the heated zone leading to the small change of the zone's radius at the same absorbed energy density.

The effects of the high- NA focusing and E-field enhanced heat conduction both lead to elongation of the focal spot in the direction of the E-field in the case of linear polarization. Semi-quantitative estimate for elongation of polymerized region could be calculated as the following. Conversion of s-pol. light to the p-pol. along the polarization direction as described above results in significant (up to 20%; see Appendix B) increase in absorption and therefore increasing the temperature gradient at the edges of the spot and promotes polymerization (cross-linking). Simultaneously, heat accumulation is also present due to the difference in the number of pulses per spot along the scan. The discussed optical and thermal mechanisms are efficient during the pulse time only. The elongation of the polymerized region might be estimated as the distance which the heat wave travels during the pulse time transferring the energy to the area unaffected by laser directly, $L_{\text{heat}} = \sqrt{D\tau} \simeq 5.5$ nm per pulse. The effect from many consecutive pulses then accumulates in a qualitative agreement with observations. It follows that the additional polymerization length directly depends on the laser fluence, wavelength, pulse duration and repetition rate: $\Delta W \propto \tau\sqrt{I\lambda}$ (Appendix. C).

Polarisation effects are ubiquitous among earlier results on ablation,²⁶ nano-ripple formation (including using relatively low $NA = 0.1 - 0.25$),⁴²⁻⁴⁴ growth of nano-flakes in solution,²² and controlled melting of films.²⁴ Elongation of fabricated features beyond extent of the focal spot is clearly shown using short laser pulses. Even at low- $NA = 0.25$ focusing and ablation of MgF_2 at very high intensity²⁵ there is clear elongation in direction of linear polarisation which is comparable in size with ablation pits for the $\tau = 1$ ps duration and $\lambda = 6.25\mu\text{m}$ wavelength pulses.

By controlling light energy delivery and absorption via polarisation control described above, new opportunities to exercise nanoscale precision in 3D polymerisation/printing are opened. Next, a photonic crystal (PhC) structure was polymerised for the angular filtering and collimation of light.⁴⁵ For such filters, polarisation induced linewidth non-homogeneity causes spatially asym-

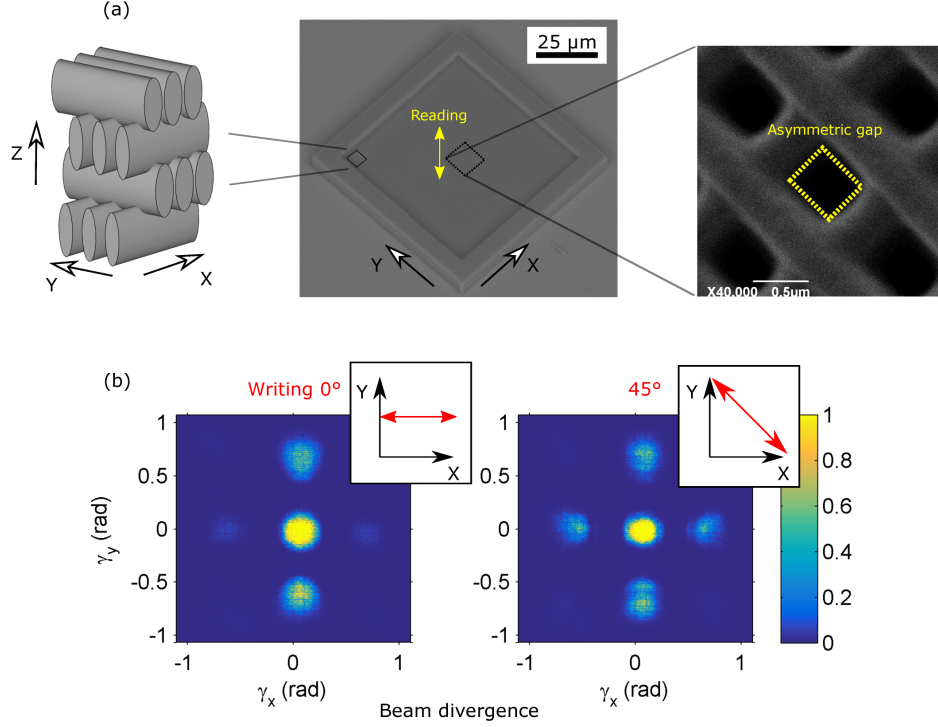


Figure 3: (a) SEM image of a woodpile PhC fabricated with two spatial periods, $d_{xy} = 1$ and $d_z = 6 \mu\text{m}$ (2 full periods, 8 layers); for a similar arrangement, see ref.⁴⁵ Galvanometric scanner was used for PhC polymerization and a monolithic wall was made to reduce deformations. Writing parameters were: the pulse energy $E_p = 0.73 \text{ nJ}$ (corresponding to $I_p = 1 \text{ TW/cm}^2$ intensity). The line width difference in respect to each other due to polarization is 8% resulting in an asymmetric gap shown in top right. (b) shows diffraction pattern obtained by focusing (NA = 0.25) a Gaussian He-Ne probe ($\lambda = 633 \text{ nm}$) on the PhC and projecting the resulting pattern on a screen (a reference grid artifact can be seen). An asymmetrical diffraction pattern for the DLW polarization oriented along the PhC X-axis is clearly recognizable on the left side whereby it is symmetrical if pre-compensated by writing direction on the right side.

metric performance of PhC structures quantifiable by angular divergence in x- and y-directions, $\gamma_{x,y}$. Figure 3 shows the PhC structure and its performance as collimating filter. Asymmetry in diffraction pattern (b) is a signature of the $\sim 10\%$ line width difference (which is enough for the clear observation) when x- linearly polarised laser beam was scanned along x- and y-directions when compared with $\pi/4$ -tilted beam which makes the same angle with the scan direction.

The proposed analysis can qualitatively explain the action of linear polarized light on the width and symmetry of the 3D suspended polymerized bridges and PhCs under tight focusing. It is shown that polarization of incident laser field allows controlling the polymerization process on a scale of

nanometers on already sub-wavelength 3D patterns.

Heat diffusion is reduced along the linear polarization and causes local over-heating but does not affect heat flow in the perpendicular direction during the pulse. Absorption is larger for the p-pol. which contributes to elongation of the polymerized features. The observed effect should be more pronounced for longer wavelengths, higher pulse energies, and longer pulses according to $\Delta W \propto \tau \sqrt{I\lambda}$. The coupling between the \mathbf{E} and ∇T is explained for the first time and provides new dimension to control optically nanoscale processes. The ascribed findings demonstrate that the beam's polarization can be practically used as the voxel's aspect ratio tuning parameter and should be taken into account for precise 3D fabrication of nanostructures such as PhCs and micro-optical components, yet perhaps can be disregarded for some bulkier objects or larger scale scaffolds.

Experimental

SZ2080 organic-inorganic hybrid material was doped with 4,4'-bis(diethylamino)-benzophenone (BIS) photoinitiator at 1% by weight and was used as a photopolymer (IESL-FORTH).⁴⁶ A drop of photosensitive material was heated for 20 min at each of 40, 70, and 90°C temperatures as a prebake prior to laser polymerization. A femtosecond Yb:KGW laser amplifier (Pharos, Light Conversion Ltd.) radiation was used at a central wavelength $\lambda = 1030$ nm with pulse repetition rate $R_{\text{rep}} = 200$ kHz and pulse duration $\tau = 300$ fs. We used middle range pulse energies from an empirically established fabrication window when 3D suspended bridges without structural damage are retrieved. This corresponded to the 1.75 mW of average optical power (measured before the objective) resulting in the 1.16 TW/cm² intensity/irradiance at the focus of a 100 \times magnification objective lens of numerical aperture $NA = 1.4$; transmission of the optical elements was taken into account. The diameter of the collimated beam coming to the objective was of 8.5 mm and the entrance aperture was 6 mm, thus an Airy disk at the focus in the sample could be observed.

During fabrication the samples were translated at a 100 $\mu\text{m/s}$ linear velocity commonly used in DLW 3D nanolithography.^{1-3,6,33,34,46} After fabrication samples were developed for 30 min in 4-methyl-2-pentanone bath and critical point drier was employed to avoid structural changes due to capillary forces. All of the samples were coated with 20 nm thick layer of gold using sputter coater (note, the actual thickness of Au

on the 3D suspended bridges was smaller). Width and height of 3D suspended lines were examined using scanning electron microscopy (SEM).

Acknowledgement

NATO SPS-985048 "*Nanostructures for Highly Efficient Infrared Detection*" grant is acknowledged.

References

1. Kawata, S.; Sun, H.-B.; Tanaka, T.; Takada, K. Finer features for functional microdevices. *Nature* **2001**, *412*, 697 – 698.
2. Lee, K.; Yang, D.-Y.; Park, S. H.; Kim, R. H. Recent developments in the use of two-photon polymerization in precise 2D and 3D microfabrications. *Polym. Adv. Technol.* **2006**, *17*, 72–82.
3. Maruo, S.; Fourkas, J. Recent progress in multiphoton microfabrication. *Laser Photon. Rev.* **2008**, *2*, 100–111.
4. Juodkazis, S.; Mizeikis, V.; Seet, K. K.; Miwa, M.; Misawa, H. Two-photon lithography of nanorods in SU-8 photoresist. *Nanotechnol.* **2005**, *16*, 846 – 849.
5. Fischer, J.; Wegener, M. Three-dimensional optical laser lithography beyond the diffraction limit. *Laser Photon. Rev.* **2013**, *7*, 22–44.
6. Kabouraki, E.; Giakoumaki, A.; Danilevicius, P.; Gray, D.; Vamvakaki, M.; Farsari, M. Redox Multi-photon Polymerization for 3D Nanofabrication. *Nano Lett.* **2013**, *13*, 3831–3835.
7. Malinauskas, M.; Farsari, M.; Piskarskas, A.; Juodkazis, S. Ultrafast-laser micro/nano-structuring of photo-polymers: a decade of advances. *Phys. Rep.* **2013**, *533*, 1–31.
8. Takada, K.; Wu, D.; Chen, Q.-D.; Shoji, S.; Xia, H.; Kawata, S.; Sun, H.-B. Size-dependent behaviors of femtosecond laser-prototyped polymer micronanowires. *Opt. Lett.* **2009**, *34*, 566–568.

9. Malinauskas, M.; Bičkauskaitė, G.; Rutkauskas, M.; Paipulas, D.; Purlys, V.; Gadonas, R. Self-polymerization of nano-fibres and nano-membranes induced by two-photon absorption. *Lith. J. Phys.* **2010**, *50*, 135–140.
10. Liu, D.-X.; Sun, Y.-L.; Dong, W.; Yang, R.-Z.; Chen, Q.-D.; Sun, H.-B. Dynamic laser prototyping for biomimetic nanofabrication. *Laser Photon. Rev.* **2014**, *8*, 882–888.
11. Jiang, L.; Zhou, Y.; W.X.; Gao, Y.; Huang, X.; Jiang, L.; Baldacchini, T.; Silvain, J.-F.; Lu, Y. Two-photon polymerization: investigation of chemical and mechanical properties of resins using Raman microspectroscopy. *Opt. Lett.* **2014**, *39*, 3034–3037.
12. Žukauskas, A.; Matulaitienė, I.; Paipulas, D.; Niaura, G.; Malinauskas, M.; Gadonas, R. Tuning the refractive index in 3D direct laser writing lithography: towards GRIN microoptics. *Laser Photon. Rev.* **2015**, *9*, 706–712.
13. Nicoletti, E.; Bulla, D.; Luther-Davies, B.; Gu, M. Generation of $\lambda/12$ Nanowires in Chalcogenide Glasses. *Nano Lett.* **2011**, *11*, 4218–4221.
14. Baldacchini, T.; Snider, S.; Zadayan, R. Two-photon polymerization with variable repetition rate bursts of femtosecond laser pulses. *Opt. Express* **2012**, *20*, 29890–29899.
15. Mueller, J.; Fischer, J.; Mange, Y.; Nann, T.; Wegener, M. In-situ local temperature measurement during three-dimensional direct laser writing. *Appl. Phys. Lett.* **2013**, *103*, 123107.
16. Sun, H.; Kawata, S. *Two-Photon Photopolymerization and 3D Lithographic Microfabrication*; Springer-Verlag, Berlin, 2004.
17. Sun, H.-B.; Maeda, M.; Takada, K.; Chon, J.; Gu, M.; Kawata, S. Experimental investigation of single voxels for laser nanofabrication via two-photon photopolymerization. *Appl. Phys. Lett.* **2003**, *83*, 819.
18. Cheng, Y.; Zeng, H.; Trull, J.; Cojocaru, C.; Malinauskas, M.; Jukna, T.; Wiersma, D.; Staliunas, K. Beam focalization in reflection from flat dielectric subwavelength gratings. *Opt. Lett.* **2014**, *39*, 6086–6089.

19. Buchegger, B.; Kreutzer, J.; Plochberger, B.; Wollhofen, R.; Sivun, D.; Jacak, J.; Schuetz, G.; Schubert, U.; Klar, T. Stimulated Emission Depletion Lithography with Mercapto-Functional Polymers. *ACS Nano* **2016**, *10*, 1954–1959.
20. Fischer, J.; Wegener, M. Three-dimensional direct laser writing inspired by stimulated-emission-depletion microscopy. *Opt. Mat. Express* **2011**, *2*, 614–624.
21. Wollhofen, R.; Katzmann, J.; Hrelescu, C.; Jacak, J.; Klar, T. 120 nm resolution and 55 nm structure size in STED-lithography. *Opt. Express* **2013**, *21*, 10831–10840.
22. Xu, B. B.; Wang, L.; Ma, Z. C.; Zang, R.; Chen, Q. D.; Lv, C.; Han, B.; Xiao, X. Z.; Zhang, X. L.; Zhang, Y. L. et al. Surface-Plasmon-Mediated Programmable Optical Nanofabrication of an Oriented Silver Nanoplate. *ACS Nano* **2014**, *8*, 6682–6692.
23. Xiong, W.; Liu, Y.; Jiang, L.; Zhou, Y.; Li, D.; Jiang, L.; Silvain, J.-F.; Lu, Y. Laser-Directed Assembly of Aligned Carbon Nanotubes in Three Dimensions for Multifunctional Device Fabrication. *Adv. Mater.* **2016**, 10.1002/adma.201505516.
24. Öktem, B.; Pavlov, I.; Ilday, S.; Kalaycoğlu, H.; Rybak, A.; Yavas, S.; Erdoğan, M.; Ilday, F. O. Non-linear laser lithography for indefinitely large area nanostructuring with femtosecond pulses. *Nature Photon.* **2013**, *7*, 897 – 901.
25. Simanovskii, D.; Schwettman, H. A.; Lee, H.; Welch, A. J. Midinfrared Optical Breakdown in Transparent Dielectrics. *Phys. Rev. Lett.* **2003**, *91*, 107601.
26. Guay, J. M.; Villafranca, A.; Baset, F.; Popov, K.; Ramunno, L.; Bhardwaj, V. R. Polarization-dependent femtosecond laser ablation of poly-methyl methacrylate. *New J. Phys.* **2012**, *14*, 085010.
27. Buividas, R.; Mikutis, M.; Juodkasis, S. Surface and bulk structuring of materials by ripples with long and short laser pulses: recent advances. *Prog. Quant. Electron.* **2014**, *38*, 119–156.
28. Temnov, V. V.; Sokolowski-Tinten, K.; Zhou, P.; El-Khamhawy, A.; von der Linde, D. Multiphoton Ionization in Dielectrics: Comparison of Circular and Linear Polarization. *Phys. Rev. Lett.* **2006**, *97*, 237403.

29. Gamaly, E.; Juodkazis, S.; Mizeikis, V.; Misawa, H.; Rode, A.; Krolokowski, W. Modification of refractive index by a single fs-pulse confined inside a bulk of a photo-refractive crystal. *Phys. Rev. B* **2010**, *81*, 054113.
30. Gamaly, E. G. The physics of ultra-short laser interaction with solids at non-relativistic intensities. *Phys. Reports* **2011**, *508*, 91 – 243.
31. Gamaly, E. G.; Rode, A. V. Physics of ultra-short laser interaction with matter: From phonon excitation to ultimate transformations. *Progr. Quant. Electron.* **2013**, *37*, 215–323.
32. Lifshitz, E. M.; Pitaevski, L. P. *Physical Kinetics*; Pergamon Press, Oxford, 1981.
33. Mueller, J.; Fischer, J.; Mayer, F.; Kadic, M.; Wegener, M. Polymerization Kinetics in Three-Dimensional Direct Laser Writing. *Adv. Mater.* **2014**, *26*, 6566–6571.
34. Malinauskas, M.; Žukauskas, A.; Hasegawa, S.; Hayasaki, Y.; Mizeikis, V.; Buividas, R.; Juodkazis, S. Ultrafast laser processing of materials: from science to industry. *Light: Sci. Appl.* **2016**, *5*, e16133.
35. Nasse, M. J.; Woehl, J. C. Realistic modeling of the illumination point spread function in confocal scanning optical microscopy. *J. Opt. Soc. Am. A* **2010**, *27*, 295.
36. Stuart, B. C.; Feit, M. D.; Rubenchick, A. M.; Shore, B. W.; Perry, M. D. Laser-induced damage in dielectrics with nanosecond to picosecond pulses. *Phys. Rev. Lett.* **1995**, *74*, 2248–2251.
37. Luther-Davies, B.; Rode, A.; Madsen, N.; Gamaly, E. G. Picosecond high-repetition-rate pulsed laser ablation of dielectrics: the effect of energy accumulation between pulses. *Opt. Eng.* **2005**, *44*, 051102.
38. Ovsianikov, A.; Shizhou, X.; Farsari, M.; Vamvakaki, M.; Fotakis, C.; Chichkov, B. Shrinkage of microstructures produced by two-photon polymerization of Zr-based hybrid photosensitive materials. *Opt. Express* **2009**, *17*, 2143–2148.
39. Chon, J. W. M.; Gan, X.; Gu, M. Splitting of the focal spot of a high numerical-aperture objective in free space. *Appl. Phys. Lett.* **2002**, *81*, 1576 – 1578.
40. Ze'ev, B.; Gu, M.; Shamir, J. Angular momentum and geometrical phases in tight-focused circularly polarized plane waves. *Appl. Phys. Lett.* **2006**, *89*, 241104.

41. Gibbon, P. *Short pulse laser interactions with Matter*; Imperial College Press, London, 2005.
42. Jia, T.; Chen, H.; Huang, M.; Zhao, F.; Qiu, J.; Li, R.; Xu, Z.; He, X.; Zhang, J.; Kuroda, H. Formation of nanogratings on the surface of a ZnSe crystal irradiated by femtosecond laser pulses. *Phys. Rev. B* **2005**, 72, 125429.
43. Lee, S.; Yang, D.; Nikumb, S. Femtosecond laser patterning of $Ta_{0.1}W_{0.9}O_x$ /ITO thin film stack. *Appl. Surf. Sci.* **2007**, 253, 4740–4747.
44. Graf, S.; Muller, F. Polarization-dependent generation of fs-laser induced periodic surface structures. *Appl. Surf. Sci.* **2015**, 331, 150–155.
45. Maigyte, L.; Purlys, V.; Trull, J.; Peckus, M.; Cojocar, C.; Gailevičius, D.; Malinauskas, M.; Staliunas, K. Flat lensing in the visible frequency range by woodpile photonic crystals. *Opt. Lett.* **2013**, 38, 2376–2378.
46. Ovsianikov, A.; Viertl, J.; Chichkov, B.; Oubaha, M.; MacCraith, B.; Sakellari, I.; Giakoumaki, A.; Gray, D.; Vamvakaki, M.; Farsari, M. et al. Ultra-Low Shrinkage Hybrid Photosensitive Material for Two-Photon Polymerization Microfabrication. *ACS Nano* **2008**, 2, 2257–2262.